J|A|C|S COMMUNICATIONS

Published on Web 07/16/2010

Expanding Micelle Nanolithography to the Self-Assembly of Multicomponent Core−Shell Nanoparticles

Beri N. Mbenkum,* Alejandro Díaz-Ortiz, Lin Gu, Peter A. van Aken, and Gisela Schütz

Max Planck Institute for Metals Research, Heisenbergstrasse 3, D-70569 Stuttgart, Germany

Received May 12, 2010; E-mail: mbenkum@mf.mpg.de

Abstract: Size, composition, and pattern formation are crucial elements in the fabrication of functional multicomponent nanoparticles (NPs). Self-assembly techniques provide relevant control over NP size distribution (down to a few nanometers in diameter), but more importantly, such techniques are amenable for practical applications since the resulting NPs (and arrays thereof) are programmed in the molecular structure of the precursors. Here, the diblock copolymer micelle nanolithography concept of achieving monodisperse NPs is extended to direct the synthesis of multicomponent core−shell NPs arranged in a triangular lattice. Special emphasis is set on $Co_{core}@Fe_{shell}$ and corrosion resistant $(FeCo)_{core}@Au_{shell}$ NPs. Electron microscopy analyses show a variety of core−shell geometries spanning a wide range of oxide, metal, and alloy combinations.

The most important factor in the synthesis of functional multicomponent nanoparticles (NPs) is the precise control over the architecture of the system, i.e., size, composition, structure, and pattern formation. The vast field of NP synthesis can be classified in two main architectural groups: (a) *dense* assemblies of interacting NPs and (b) *dilute* noninteracting NPs. The former profits from the fact that the constitutive NPs act as *artificial atoms*, thus creating materials that rely mainly on the collective response of the system. Such configurations serve well in photonic,[1,2] photovoltaic,[3] and energy storage systems.[4] The dilute NP scheme, on the other hand, depends on the properties and performance of the individual NPs, as in biomedical (e.g., imaging[5] and tumor therapy[6−8]) or catalytic[9] systems, where size and structure of the individual components dictate efficiency and functionality. Two-dimensional arrays of NPs on substrates provide an interesting and exciting regime where the individual and collective properties of the constitutive NPs can be exploited simultaneously. Such architectures are the cornerstone for NP-based magnetic data-storage devices,[10] biosensors,[2] as well as functional interfaces to tailor cell−matrix interaction.[11,12] In particular, the individual properties of NPs can be tailored by changing the average size and composition (alloy systems). In recent years, the latter step has been actively investigated since alloy core−shell (CS) NPs are ideal multifunctional structures; i.e., shell and core provide different, sometimes synergistic functions.[13]

The synthesis of monodisperse CS NPs is, however, challenging, typically involving successive reduction of the corresponding metal precursors,[14,15] scaling of the reduction rates of the individual materials, purification steps, implementation of ligands for NP stabilization, and, when needed, an inert atmosphere for the preparation of nonoxidized NPs.[3,9,13,14,16,17] In addition, the controlled deposition of the NPs on surfaces is far from trivial. This particular step is, however, crucial for devices such as NP-based magnetic data-storage systems. A promising avenue to control deposition of NPs on surfaces is micelle nanolithography. The strength and appeal of the micelle technique lie in its applicability to nearly any wetable (e.g., Si, Al_2O_3, etc.) large surface area. So far, the technique has mainly been used to synthesize single-component[18,19] NPs with fine control over their size (<10 nm in diameter) and lateral spacing (20−200 nm) on substrates. Initial attempts to achieve bimetallic NPs such as FePt with this technique have not reported the existence of a CS structure.[20,21] This most likely resides in the high temperature steps ($T \geq 500$ °C) incorporated in the NP processing chain premicroscopy studies which modified the overall NP architecture. Temperatures of ∼250 °C have been used in other NP systems to transit from a Co@Fe CS to FeCo alloy architecture.[22]

In this communication, we advance the diblock copolymer nanolithography approach to the self-assembly of multicomponent (binary and ternary) CS NPs on surfaces that render well-defined 2D NP arrays of tunable architecture. Our approach to achieve CS NPs is as follows: Initially, polystyrene (*x*)-*block*-poly(2-vinylpyridine)(*y*), PS-*b*-P2VP diblock copolymer (PS(1200)-b-P2VP(556), polydispersity index = 1.05, is dissolved to 4 mg/mL in toluene and stirred for 12 h. Depending on the NP architecture of interest, commercially available metal salts such as $HAuCl_4 \cdot 4H_2O$, $Co(NO_3)_2 \cdot 6H_2O$, and $Fe(NO_3)_3 \cdot 9H_2O$ are added (with defined molar ratios of each salt with respect to pyridine depending on the desired core or shell size) to the micelle solution and stirred for another 72 h. The proportion of each metal salt added to the micelle solution determines the architecture (i.e., core and shell size distribution) of the resultant NPs. All reactions proceed at room temperature and atmospheric pressure. At this point, only metal−pyridine complexes form within the micelles. A monolayer of metal-loaded micelles is obtained by spin-coating a drop of the solution at 2000 rpm on a clean dry wetable substrate. For transmission electron microscopy (TEM) samples, the solution is drop-cast on a standard Si_3N_4 TEM grid and the excess solvent is retracted with filter paper. A subsequent plasma treatment (300 W, 0.4 mbar; 60 min) etches away the micelles leaving behind CS NPs on the surface. It is worth noting that the synthesis procedure adopted here is not the classical case which involves the sequential growth of the core and shell materials.[13,14,17] Here, all salts are mixed in the micelles and the NP CS architecture self-assembles during the plasma process.

The superb magnetic properties of Fe−Co alloys and their possible implementation in biomedical[23,24] and magnetic data-storage applications[5,8,10,13] instigated our synthesis of NPs made of Fe, Co, and Au. The upper row of Figure 1 shows a schematic view of the metal-loaded micelles before plasma treatment (Figure 1a) and the corresponding multicomponent NPs obtained thereafter (Figure 1b and 1c). The corresponding scanning electron microscopy (SEM) images (45° tilted view) reveal metal-loaded micelles with average diameters $D \approx 50$ nm and projected spacings $l \approx 125$ nm, in a quasi hexagonal array (Figure 1d). SEM images of the binary (Fe−Co: $D \approx 14$ nm, $l \approx 90$ nm) and ternary

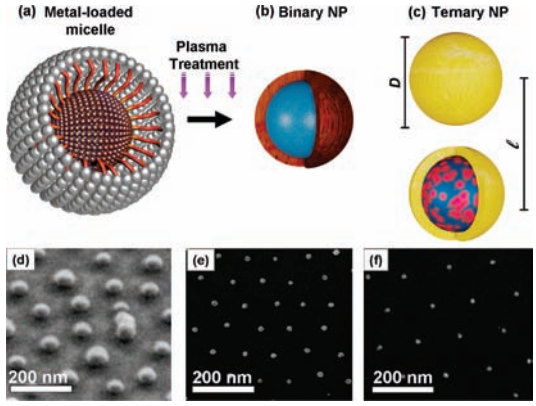

Figure 1. (a) Schematic cross section of metal-loaded micelle before plasma treatment and the obtained (b) binary and (c) ternary NPs thereafter. The corresponding SEM images of each system (d−f), respectively.

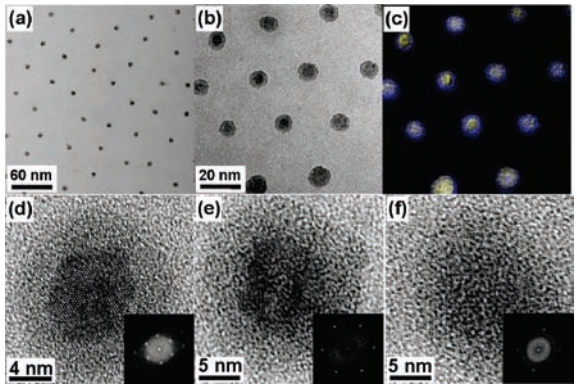

Figure 2. TEM images of the binary and ternary NPs. (a) Low-magnification profile of Fe−Co NPs, (b) bright-field zero-loss-filtered image and the corresponding elemental mapping in (c), in which Au (blue) was found surrounding Fe−Co alloys (yellow). (d) HRTEM images showing lattice details of the cores of the (d) Fe−Co and (e−f) Fe−Co@Au NPs. Fourier transforms of the HRTEM images shown in the insets (d) (core), (e) (core), and (f) (shell) indicate the Co, Fe−Co alloy cores and a Au shell of the respective NPs.

(Fe−Co−Au: $D \approx 11$ nm, $l \approx 125$ nm) NPs are shown in Figure 1e and 1f, respectively. Figure 2 shows the binary and ternary NPs as imaged by TEM. Low magnification profile and high-resolution imaging of the Fe−Co system on a Si_3N_4 TEM grid reveals a relatively ordered pattern (Figure 2a) of NPs consisting of a core with lattice constant of ~3.5 Å corresponding to fcc Co surrounded by an ~3 nm thick (most likely an oxidized Fe) shell (Figure 2d). For the ternary NPs, Figure 2b shows a bright-field zero-loss-filtered electron micrograph with the corresponding elemental mapping (Figure 2c) revealing a Au shell (blue) surrounding the Fe−Co core (yellow) structure. Fourier transforms of the HRTEM images are shown in the respective insets of Figure 2e and 2f. The 4 nm thick shell has a lattice spacing of 2.35 Å corresponding to the (111) interplane spacing of Au. The lattice constant of the core is 2.05 Å, consistent with a bcc-based Fe−Co alloy. The darker appearance of the NP core region in the TEM images is assigned to the diffraction contrast achieved when the core region is aligned to the zone axis and also is due to higher electron absorption within the core region of the NP due to the thickness of the material in comparison to the thinner peripheral shell. Control over NP architecture by scaling the proportion of the different metal salts is exemplified in Figure 3 for Fe−Co@Au NPs. The Au shell thickness was maintained at 1.7 ± 0.2 nm while the core was

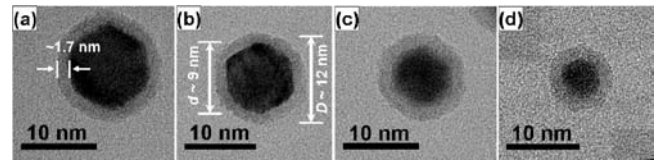

Figure 3. TEM images of Fe−Co@Au NPs with constant Au shell thickness and variable core size. The total NP diameters are $D \approx$ (a) 14, (b) 12, (c) 11, and (d) 8.5 nm. The Au shell of the NPs is 1.7 ± 0.2 nm thick.

tailored to adopt diameters of about 11, 9, 7, and 5 nm as shown in Figure 3a−3d, respectively.

This work illustrates the pertinence of the micellar technique to precisely control CS NP architecture. The stirring process enables uniform dissolution of the metal precursors into the micelle cores. The plasma treatment plays the multiple role of etching the organic constituents of the micelle film, reducing the metal ions and inducing a segregation of the individual metallic components to enable a CS architecture. The CS architecture achieved during the plasma process is rationalized to be driven by the bulk surface energies of the metallic species in the system. The respective bulk surface energies of each element are Au (1.51 J/m^2), Fe (2.42 J/m^2), and Co (2.52 J/m^2).[1] Under the self-assembly conditions within our system, it is apparently energetically favorable for the material with a higher surface energy to adopt the core position and that with a lower surface energy to adopt the peripheral one within the CS configuration. This is particularly evident in the ternary system where Au, which has a lower surface energy than both Fe and Co, adopts the peripheral position in the CS configuration. Achieving the reverse architecture, e.g. Co@Fe NPs, represents a current challenge for the technique.

In conclusion, a novel simple methodology to achieve monodisperse multicomponent CS NPs in one reduction step, with fine-tuning of the NP architectural details, has been demonstrated. The current challenge of the technique lies in the achievement of a reverse architecture (e.g., $Fe_{core}Co_{shell}$). The appealing nature of the technique nevertheless lies in the simplicity of the reaction conditions and its applicability to a vast range of material combinations. The additional asset of independently manipulating the size and lateral distribution of the NPs on surfaces provides an attractive configuration for the fundamental study of material- and size-dependent dipole interactions between NPs.[17]

Acknowledgment. The authors are grateful to E. V. Mbenkum for assistance with the 3D artwork. The technical support of P. Kopold in transmission electron microscopy is well appreciated. A.D.-O. acknowledges support from the Alexander von Humboldt Foundation. L.G. and P.A.v.A. acknowledge financial support from the European Union under the Framework 6 program under a contract for an Integrated Infrastructure Initiative. Reference 026019 ESTEEM.

Supporting Information Available: Experimental details on the TEM methods and cross-sectional HRTEM analysis of CS NP/substrate configuration. This material is available free of charge via the Internet at http://pubs.acs.org.

References

(1) Jiang, Q.; Lu, H. M. *Surf. Sci. Rep.* **2008**, *63*, 427–464.
(2) Sanchez-Iglesias, A.; Aldeanueva-Potel, P.; Ni, W. H.; Perez-Juste, J.; Pastoriza-Santos, I.; Alvarez-Puebla, R. A.; Mbenkum, B. N.; Liz-Marzan, L. M. *Nano Today* **2010**, *5*, 21–27.
(3) Talapin, D. V.; Lee, J. S.; Kovalenko, M. V.; Shevchenko, E. V. *Chem. Rev.* **2010**, *110*, 389–458.
(4) Zhong, C. J.; Luo, J.; Fang, B.; Wanjala, B. N.; Njoki, P. N.; Loukrakpam, R.; Yin, J. *Nanotechnology* **2010**, *21*, 062001.

(5) Seo, W. S.; Lee, J. H.; Sun, X. M.; Suzuki, Y.; Mann, D.; Liu, Z.; Terashima, M.; Yang, P. C.; McConnell, M. V.; Nishimura, D. G.; Dai, H. J. *Nat. Mater.* **2006**, *5*, 971–976.
(6) Habib, A. H.; Ondeck, C. L.; Chaudhary, P.; Bockstaller, M. R.; McHenry, M. E. *J. Appl. Phys.* **2008**, *103*, 07A307.
(7) Kim, D. H.; Rozhkova, E. A.; Ulasov, I. V.; Bader, S. D.; Rajh, T.; Lesniak, M. S.; Novosad, V. *Nat. Mater.* **2010**, *9*, 165–171.
(8) Polyak, B.; Fishbein, I.; Chorny, M.; Alferiev, I.; Williams, D.; Yellen, B.; Friedman, G.; Levy, R. J. *Proc. Natl. Acad. Sci. U.S.A.* **2008**, *105*, 698–703.
(9) Ferrando, R.; Jellinek, J.; Johnston, R. L. *Chem. Rev.* **2008**, *108*, 845–910.
(10) Goll, D. *Intl. J. Mater. Res.* **2009**, *100*, 652–662.
(11) Huang, J. H.; Grater, S. V.; Corbellinl, F.; Rinck, S.; Bock, E.; Kemkemer, R.; Kessler, H.; Ding, J. D.; Spatz, J. P. *Nano Lett.* **2009**, *9*, 1111–1116.
(12) Huang, J.; Ding, J. *Soft Matter* **2010**, DOI: 10.1039/b927168f.
(13) Liz-Marzan, L. M.; Mulvaney, P. *J. Phys. Chem. B* **2003**, *107*, 7312–7326.
(14) Reiss, P.; Protiere, M.; Li, L. *Small* **2009**, *5*, 154–168.
(15) Liu, P.; Ding, J. D. *Langmuir* **2010**, *26*, 492–497.
(16) Desvaux, C.; Amiens, C.; Fejes, P.; Renaud, P.; Respaud, M.; Lecante, P.; Snoeck, E.; Chaudret, B. *Nat. Mater.* **2005**, *4*, 750–753.
(17) Lu, A. H.; Salabas, E. L.; Schuth, F. *Angew. Chem., Int. Ed.* **2007**, *46*, 1222–1244.
(18) Antonietti, M.; Wenz, E.; Bronstein, L.; Seregina, M. *Adv. Mater.* **1995**, *7*, 1000–1005.
(19) Glass, R.; Moller, M.; Spatz, J. P. *Nanotechnology* **2003**, *14*, 1153–1160.
(20) Ethirajan, A.; Wiedwald, U.; Boyen, H. G.; Kern, B.; Han, L. Y.; Klimmer, A.; Weigl, F.; Kastle, G.; Ziemann, P.; Fauth, K.; Cai, J.; Behm, R. J.; Romanyuk, A.; Oelhafen, P.; Walther, P.; Biskupek, J.; Kaiser, U. *Adv. Mater.* **2007**, *19*, 406–410.
(21) Gao, Y.; Zhang, X. W.; Yin, Z. G.; Qu, S.; You, J. B.; Chen, N. F. *Nanoscale Res. Lett.* **2010**, *5*, 1–6.
(22) Wang, C.; Peng, S.; Lacroix, L. M.; Sun, S. H. *Nano Res.* **2009**, *2*, 380–385.
(23) Kline, T. L.; Xu, Y. H.; Jing, Y.; Wang, J. P. *J. Magn. Magn. Mater.* **2009**, *321*, 1525–1528.
(24) Xu, Y. H.; Wang, J. P. *Appl. Phys. Lett.* **2007**, *91*, 233107.

JA104098U